

## Diffusion-limited aggregation as a Markovian process: Bond-sticking conditions

Boaz Kol and Amnon Aharony

*Raymond and Beverly Sackler Faculty of Exact Sciences, School of Physics and Astronomy,  
Tel Aviv University, 69978 Ramat Aviv, Israel*

(Received 14 February 2000)

Cylindrical lattice diffusion limited aggregation (DLA), with a narrow width  $N$ , is solved using a Markovian matrix method. This matrix contains the probabilities that the front moves from one configuration to another at each growth step, calculated exactly by solving the Laplace equation and using the proper normalization. The method is applied for a series of approximations, which include only a finite number of rows near the front. The matrix is then used to find the weights of the steady-state growing configurations and the rate of approaching this steady-state stage. The former are then used to find the average upward growth probability, the average steady-state density and the fractal dimensionality of the aggregate, which is extrapolated to a value near 1.64.

PACS number(s): 61.43.Hv, 05.20.Dd, 02.50.Ga

### I. INTRODUCTION

Diffusion-limited aggregation (DLA) [1] has been the subject of extensive study since it was first introduced. This model exhibits a growth process that produces highly ramified self similar patterns, which are believed to be fractals [2]. It seems that DLA captures the essential mechanism in many natural growth processes, such as viscous fingering [3], dielectric breakdown [4], etc. It is now understood that the Laplace equation, which is common to all of these processes and to DLA, has a major role in the resemblance between them. One of the interesting features of DLA is that there are no parameters to fine-tune in order to obtain a fractal. It thus differs from ordinary critical phenomena, and belongs to the class of self-organized criticality (SOC) [5]. In spite of the apparent simplicity of the model, an analytic solution is still unavailable. Particularly, the exact value of the fractal dimension is not known. Some of the analytic approaches employed so far include the fixed scale transformation (FST) [6], real space renormalization group (RSRG) [7–9] and conformal mapping [10,11].

In DLA there is a seed cluster of particles fixed somewhere. A particle is released at a distance from the cluster, and performs a random walk until it attempts to penetrate the fixed cluster, in which case it sticks. Then the next particle is released and so on. There are two common types of sticking conditions. The sticking condition described above is called ‘‘bond-DLA,’’ because it occurs when a particle goes into a perimeter bond. In ‘‘site-DLA,’’ sticking occurs as soon as the particle arrives in a perimeter site. This paper deals with bond-DLA, whereas site-DLA will be considered elsewhere [12]. The large scale structure of DLA is not sensitive to the type of sticking conditions used [13].

It has been shown that bond-DLA is equivalent to the dielectric breakdown model (DBM) with  $\eta=1$  [4,14]. DBM is a cellular automaton that is defined on a lattice. It consists of the following steps: one starts with a seed cluster of connected sites and with a boundary surface far away from it. A field  $\Phi$ , which corresponds to the electrostatic potential, is found by solving the discrete Laplace equation on a lattice,

$$\nabla^2\Phi=0, \quad (1.1)$$

with the following boundary conditions: the aggregate is considered to have a constant potential that is usually set to 0, and the potential gradient on the distant boundary is set to 1 in some arbitrary units (some use a constant potential on the distant boundary instead). In this paper we set the distant boundary at infinity, and ignore the exponentially small finite size corrections. After solving the discrete Laplace equation (1.1), the field  $\Phi$  determines the growth probabilities per perimeter bond. More specifically, the growth probabilities are proportional to the electric field to some power  $\eta$ . The electric field is simply equal to the potential difference across each bond. Because the potential is set to 0 on the aggregate, the electric field is equal to the potential value at the sites lying across the perimeter bonds. Thus,

$$P_b = \frac{|\Phi_b|^\eta}{\sum_b |\Phi_b|^\eta}. \quad (1.2)$$

Here,  $b$  is the bond index.

DLA and DBM can be grown in various geometries. By geometry we refer to the dimensionality of the lattice, to the shapes of the boundaries and to the details of the seed for growth (usually a point or a line for two-dimensional growth). For instance, the case in which the distant boundary is a sphere is called radial boundary conditions, and the case in which the boundary is a distant plane at the top, while the seed cluster is a parallel plane at the bottom, with periodic boundary conditions on the sides, is called cylindrical boundary conditions. In this paper we only consider the cylindrical case, with a relatively short period length (width), from  $N=2$  to about  $N=7$ , although the method described here could also be used for wider cases.

Recently we published an exact solution to DLA in cylindrical geometry of width  $N=2$  [15]. The present paper generalizes and extends that solution. Our approach follows the dynamics of the interface. The interface alone determines the growth probabilities at each time step, and whatever lies

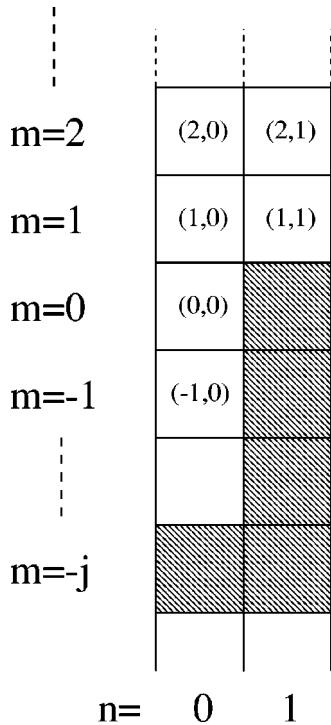


FIG. 1. The coordinates  $(m,n)$  describe the location on a lattice that is two sites wide. The gray sites belong to the interface of the aggregate, which is shaped as a step of size  $j$ .

behind it is irrelevant. This is because the solution to the Laplace equation is unique, provided that the boundary conditions are well defined. We now give a brief summary of Ref. [15]. The characterization of the interface for  $N=2$  is simple; the interface is *fully* characterized by a single parameter (usually denoted by  $i$  or  $j$ ), which corresponds to the height difference between the two columns. This height difference, referred to as the step size, can be infinitely large; see Fig. 1. If the interface is flat ( $j=0$ ), one can assume that the next particle will always stick on the right side, without limiting the generality of this discussion. This means that the step size can always be considered as non-negative. The Markovian dynamics is then presented using the Master equation,

$$P_i(t+1) = \sum_{j=0}^{\infty} E_{i,j} P_j(t), \quad (1.3)$$

where  $P_j(t)$  is the probability that the step size is  $j$  at time  $t$ , and  $E_{i,j}$  is the time independent conditional probability that an initial step size  $j$  will become  $i$  after the next growth process. An example with several possible transitions is shown in Fig. 2.  $\mathbf{P}(t)$  is called the state vector and  $\mathbf{E}$  is called the evolution matrix. In principle, a similar Master equation can be written for more complex growth situations, provided the various configurations can be indexed with a single index  $j$ . Being made out of conditional probabilities, the elements of the evolution matrix obey that,

$$0 \leq E_{i,j} \leq 1, \quad i, j = 0, \dots, \infty,$$

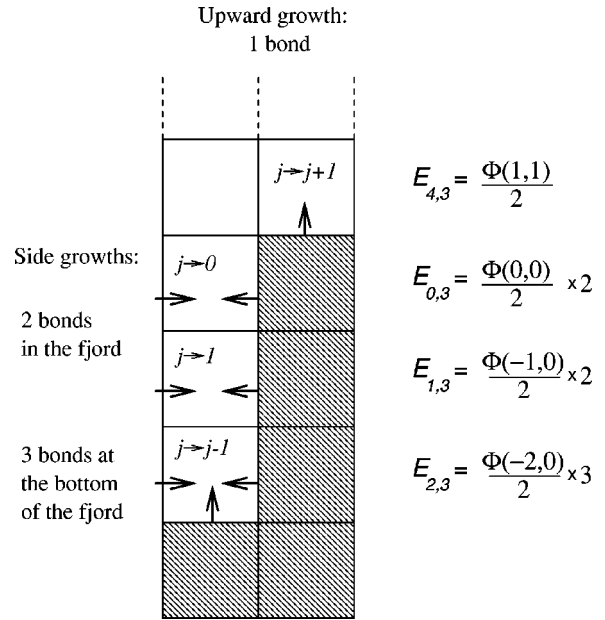


FIG. 2. Possible growth processes that change the interface from an initial step size  $j=3$  to a final size  $i=4,0,1,2$ . The growth probability is determined by the potential and the number of bonds associated with the site where growth is to occur.  $E_{i,j}$  is the conditional probability to grow from an initial step size  $j$  to a final step size  $i$ . The normalization follows from Eq. (1.10).

$$\sum_{i=0}^{\infty} E_{i,j} = 1, \quad j = 0, \dots, \infty. \quad (1.4)$$

After many iterations of Eq. (1.3) the system converges to a fixed point  $\mathbf{P}^*$ , also called the steady state, which represents the asymptotic time distribution of the step sizes. From the steady state and the evolution matrix we are able to extract the average upward growth probability  $\langle p_{\text{up}} \rangle^*$ , the average density  $\rho$  and the fractal dimension  $D$ .

In order to obtain an analytic expression for the elements of the evolution matrix, one must first solve the Laplace equation. Having found the solutions  $\Phi(m,n)$ , the growth probabilities are found from Eq. (1.2). The denominator there, which comes from the normalization, is particularly simple for the special case of  $\eta=1$ , where the discrete version of the divergence theorem implies that [15]

$$\sum_b \Phi_b = N. \quad (1.5)$$

The actual growth probability into a site is then found from

$$p_{\text{site}} = \sum_{\text{bonds into site}} p_b. \quad (1.6)$$

The solution of the Laplace equation is now divided into two parts. In the first part, we solve the Laplace equation for the “upper” part of space, which starts just above the highest particle of the aggregate and continues upwards to infinity. In the example of Fig. 1, this part contains all the rows with  $m \geq 0$ . As we explain below, this solution is completely determined by the boundary conditions and by the values of the potential at the row with  $m=0$ , i.e.,  $\{\Phi(0,n)\}$ . We then

solve the Laplace equation for the “lower” part ( $m \leq 0$  in Fig. 1), and find the values of  $\{\Phi(0, n)\}$  from matching the two regimes. The solution in the “upper” part is given as a combination of solutions of the form [15]

$$\Phi(m, n) = e^{\kappa m + i k n}, \quad (1.7)$$

with the dispersion relation

$$\sinh\left(\frac{\kappa}{2}\right) = \pm \sin\left(\frac{k}{2}\right) \quad (1.8)$$

and with the discrete set of allowed values  $k_l = (2\pi/N)l$ , which follow from the periodic lateral boundary conditions, which require that  $e^{i k N} = 1$ . The boundary conditions at infinity have a uniform gradient, i.e.,

$$\lim_{m \rightarrow \infty} [\Phi(m+1, n) - \Phi(m, n)] = 1, \quad n = 0, \dots, N-1. \quad (1.9)$$

Given the arbitrarily set of values  $\Phi(0, n)$ , the solution for the row  $m = 1$  is

$$\Phi(1, n) = 1 + \sum_{n'=0}^{N-1} \Phi(0, n') g_N(|n - n'|), \quad (1.10)$$

where

$$g_N(n) \equiv \frac{1}{N} \sum_{l=0}^{N-1} e^{-\kappa_l n} \cos(k_l n), \quad n = 0, \dots, N-1, \quad (1.11)$$

is the boundary Green's function, and  $\kappa_l$  corresponds to  $k_l$  via the dispersion relation (1.8). The solution is given only for  $m = 1$ , because we are only interested in the potential at sites near the interface. Note that the Green's function has the general property

$$\sum_{n=0}^{N-1} g_N(n) = 1 \quad (1.12)$$

[15]. It is therefore good practice to check this normalization for each of the calculations presented below. Indeed, all our results obey this rule.

In general, the solution in the “lower” regime is complicated by the variety of configurations. However, this solution is very simple for  $N = 2$ , when  $\Phi(m, 0)$  is a linear combination of  $e^{\kappa_f m}$  and  $e^{-\kappa_f m}$ . Since  $\Phi(-j, 0) = 0$ , one is left with one unknown  $\Phi(0, 0)$ , to be determined by the matching at row 0.

For the special case  $N = 2$ , the above procedure has led to the exact solution [15]

$$E_{i,j} = \begin{cases} y(\infty) e^{-\kappa_f i} \frac{1 - e^{-2\kappa_f(j-i)}}{1 + \beta e^{-2\kappa_f j}}, & 0 \leq i \leq j-2 \\ \frac{3}{2} y(\infty) e^{-\kappa_f(j-1)} \frac{1 - e^{-2\kappa_f}}{1 + \beta e^{-2\kappa_f j}}, & i = j-1 \\ E_{\infty+1, \infty} \left( 1 - \alpha \frac{e^{-2\kappa_f j}}{1 + \beta e^{-2\kappa_f j}} \right), & i = j+1 \\ 0 & \text{otherwise,} \end{cases} \quad j \geq 1, \quad (1.13)$$

where

$$E_{\infty+1, \infty} = \lim_{j \rightarrow \infty} E_{j+1, j} = \frac{1 + g_2(1) y(\infty)}{2} = 0.5658 \dots, \quad (1.14)$$

$y(\infty) = \sqrt{3} - \sqrt{2} = 0.3178 \dots$ ,  $e^{-\kappa_f} = 2 - \sqrt{3} = 0.2679 \dots$ ,  $\alpha = (1 + \beta) g_2(1) y(\infty) / (2 E_{\infty+1, \infty}) = 0.1281 \dots$  and  $\beta = 5 - \sqrt{24} = 0.1010 \dots$ . For  $j = 0$ , the interface will transform into a step of size  $j = 1$  with probability 1, hence  $E_{1,0} = 1$  and  $E_{i,0} = 0$  for  $i \neq 1$ . The values of  $E_{i,j}$  for  $0 \leq i, j \leq 4$ , up to the fourth decimal digit, are

$$\mathbf{E} = \begin{bmatrix} 0 & 0.4393 & 0.3160 & 0.3177 & 0.3178 & \dots \\ 1 & 0 & 0.1185 & 0.0847 & 0.0851 & \\ 0 & 0.5607 & 0 & 0.0318 & 0.0227 & \\ 0 & 0 & 0.5655 & 0 & 0.0085 & \\ 0 & 0 & 0 & 0.5658 & 0 & \\ \vdots & & & & & \ddots \end{bmatrix}. \quad (1.15)$$

The first diagonal below the main, which represents the probabilities for the step to grow larger by one,  $E_{j+1, j}$ , approaches its asymptotic value of  $E_{\infty+1, \infty} = 0.5658 \dots$  exponentially, as the third row of Eq. (1.13) indicates. The diagonal above the main represents the probabilities for growths at the bottom of the fjord,  $E_{j-1, j}$ , and corresponds to the second row in Eq. (1.13). These probabilities decay exponentially as the step size  $j$  grows. According to the first row in Eq. (1.13), the elements  $E_{i, j}$  converge exponentially for large  $j$ 's to a simple exponential function,

$$E_{i, \infty} = \lim_{j \rightarrow \infty} E_{i, j} = y(\infty) e^{-\kappa_f i}. \quad (1.16)$$

These probabilities relate to the transition from a very large step to a step of size  $i$ . Next, the steady-state vector  $\mathbf{P}^*$  is computed and used to evaluate the average upward growth probability  $\langle p_{\text{up}} \rangle^*$ , which in turn, determines the average density  $\rho$  and the fractal dimension  $D$ . These computations are explained later in Sec. II.

Our previous paper does not specify details concerning the manner in which the system converges to the steady state in time. Besides addressing this issue, our present paper also treats DLA grown in wider geometrical periods (still in cy-

TABLE I. The two-dimensional approximate results for various channel widths  $N$  and for different orders of approximation  $O$ . The quantities presented in each table cell are the average upward growth probability  $\langle p_{\text{up}} \rangle^*$  and the number of configurations  $N_c$ . The approximate results are compared with simulations.

$N/O$	Simulation	1	2	3	4	5	6
3	0.5462	0.569 489	0.545 911	0.546 046	0.546 126	0.546 132	0.546 132
		3	7	17	45	127	371
4	0.4657	0.495 435	0.464 571	0.465 395	0.465 730	0.465 765	0.465 768
		5	20	98	575	3640	23 676
5	0.4106	0.444 088	0.407 582	0.409 497	0.410 414	0.410 547	
		7	47	457	5539	69 791	
6	0.3696	0.405 619	0.364 352	0.367 295	0.369 172		
		12	131	2217	49 678		
7	0.3377	0.375 448	0.330 112	0.333 622			
		17	337	10 403			

lindrical geometry). The basic approach is the same, i.e., we try to characterize the possible configurations of the interface for wider periods, and then write the evolution matrix, which is composed of the growth probabilities, which are computed from the Laplace potential, after proper normalization. The first difficulty encountered is in the characterization. For example, already for a width of  $N=3$  one cannot characterize the interface using a single parameter as in the case  $N=2$ , nor is it easy doing so using two parameters, or more. Instead, we make a manual list of possible configurations of the interface, which we then order according to the difference in height between the highest and lowest points on the interface. This difference is denoted by  $\Delta m$ . Our order- $O$  approximation includes only the configurations with  $\Delta m \leq O$ . In our approximation, some of these configurations represent many other (excluded) configurations, in the sense that they have very similar growth probabilities, especially upward. This is because of the screening quality of the Laplace equation, which causes the potential to decay exponentially inside fjords. Thus, the deeper parts of the interface have a very small effect on the upward growth probability. The finite list of configurations is indexed arbitrarily, with an index usually denoted by  $i$  or  $j$ . Our experience shows that accurate results are obtained, only when the order of approximation  $O$  is comparable to the width of the cylinder  $N$ . Thus, for wide periods, a high-order calculation is called for. This causes the method to be ineffective for very wide periods, because the number of configurations grows exponentially with the order of approximation. We conducted calculations up to  $N=7$ .

After selecting the finite list of configurations and obtaining the finite evolution matrix, we compute the steady-state vector, which is the fixed point of the matrix (the normalized eigenvector with an eigenvalue of 1). For each configuration, we identify the upward growth processes (when the newly attached particle is higher than the rest). We then calculate the average upward growth probability  $\langle p_{\text{up}} \rangle^*$  as a weighted average over the configurations. From  $\langle p_{\text{up}} \rangle^*$  we calculate the average density  $\rho$  and the fractal dimension  $D$ . The computed values of  $\langle p_{\text{up}} \rangle^*$ , from different orders of the approximation, are compared with numerical simulations in Table I.

In Sec. II we introduce a simple Markov process, called the ‘‘frustrated climber,’’ which we solve exactly. A slight modification of the model is equivalent to site-DLA with a period of  $N=2$ , which is presented elsewhere [12]. We then

show a way of successively generalizing the model to approximate bond-DLA with a period of  $N=2$  and with increasing orders  $O$ . We are able to check the approximations by comparing with the exact results of Ref. [15]. This model also enables us to investigate the rate of convergence to the steady state. In this context we describe the convergence in terms of other eigenvectors, with eigenvalues whose absolute values are smaller than 1, and in terms of the infinite shift-down operator. We show that the average upward growth probability converges exponentially in time to its steady-state value, with a characteristic time constant on the order of unity. In Sec. III we generalize our method to cylindrical DLA with  $N>2$ . We present in detail the calculations for  $N=3$  with  $O=1$  and  $O=2$ , and for  $N=4$  with  $O=1$ . Next we report on numerical results for wider periods and higher orders. In the final section we review the results and summarize.

## II. FRUSTRATED CLIMBER MODEL

Consider someone trying to climb up a slippery infinite ladder. At each time step the climber climbs up one step with probability  $0 \leq p \leq 1$ , or falls all the way down with probability  $q \equiv 1-p$ . We call the climber ‘‘frustrated,’’ because the probability to get very high is exponentially small. We wish to compute the probability  $P_i(t)$  for the climber to be at height  $i$  after  $t$  time steps, for  $i=0, \dots, \infty$ . The Master equation for this problem is  $\mathbf{P}(t+1) = \mathbf{E}\mathbf{P}(t)$ , where the matrix element  $E_{i,j}$  is the conditional probability that the climber moves from height  $j$  to  $i$  in a single time step. The rules of the model imply that

$$E_{i,j} = \begin{cases} p, & i=j+1 \\ q, & i=0, \quad j \geq 0, \\ 0, & \text{otherwise} \end{cases} \quad (2.1)$$

so the matrix looks like this,

$$\mathbf{E} = \begin{bmatrix} q & q & q & q & \cdots \\ p & 0 & 0 & 0 & \\ 0 & p & 0 & 0 & \\ 0 & 0 & p & 0 & \\ \vdots & & & & \ddots \end{bmatrix}. \quad (2.2)$$

This presentation helps us see the resemblance to the dynamics of DLA with  $N=2$  in Eqs. (1.13), (1.15): Eq. (2.2) would approximate these equations if we were to replace  $E_{j+1,j}$  by  $p \approx E_{\infty+1,\infty}$  and  $E_{0,j}$  by  $q$  for all  $j$ , and neglect all other growth probabilities, which are indeed smaller. We shall discuss this and better approximations for DLA in the next subsections. Because the Markovian matrices for the two cases are similar for large  $j$ 's, we expect that some of the dynamical features are similar as well. We therefore present here an exact solution for the frustrated climber model, and then try to draw conclusions for generalized models which represent successive approximations for DLA. The advantage is that in the simple model of the frustrated climber it is possible to derive a simple analytic expression for the steady state and a complete description of the temporal convergence.

The steady-state equations for the frustrated climber model are

$$P_{i+1}^* = \sum_{j=0}^{\infty} E_{i+1,j} P_j^* = p P_i^*, \quad i \geq 0, \quad (2.3)$$

$$\Rightarrow P_j^* = q p^j, \quad j \geq 0. \quad (2.4)$$

One can easily check that this steady state is normalized,

$$\sum_{j=0}^{\infty} P_j^* = \sum_{j=0}^{\infty} q p^j = \frac{q}{1-p} = 1. \quad (2.5)$$

The average upward growth probability in the steady state is

$$\langle p_{\text{up}} \rangle^* = \sum_{j=0}^{\infty} P_j^* p_{\text{up}}(j) = \sum_{j=0}^{\infty} P_j p = p, \quad (2.6)$$

where  $p_{\text{up}}(j)$  stands for the probability to move upwards when the height of the climber is  $j$ . In this simple model  $p_{\text{up}}(j) = p$  for all  $j$ 's.

We now investigate the temporal convergence to the steady state. We define the vector  $\mathbf{v}(t)$  by

$$\mathbf{P}(t) = \mathbf{P}^* + \mathbf{v}(t). \quad (2.7)$$

Because  $\mathbf{P}^*$  and  $\mathbf{P}(t)$  are probability vectors,  $\sum_{j=0}^{\infty} P_j^* = \sum_{j=0}^{\infty} P_j(t) = 1$ , for any  $t$ , hence

$$\sum_{j=0}^{\infty} v_j(t) = 0. \quad (2.8)$$

We substitute  $\mathbf{v}$  into the dynamical equation and obtain

$$\mathbf{P}(t+1) = \mathbf{E}\mathbf{P}(t) = \mathbf{P}^* + \mathbf{E}\mathbf{v}(t), \quad (2.9)$$

$$\Rightarrow \mathbf{v}(t+1) = \mathbf{E}\mathbf{v}(t). \quad (2.10)$$

Next, we look for the rest of the eigenvectors of the evolution matrix [any eigenvector  $\mathbf{v}$  with an eigenvalue  $\lambda \neq 1$ , has to obey Eq. (2.8)]. Surprisingly, there are no eigenvectors besides the steady state in this case. The eigenvector equations are

$$\lambda v_0 = q \sum_{j=0}^{\infty} v_j = 0,$$

$$\lambda v_{i+1} = p v_i(t), \quad i \geq 0. \quad (2.11)$$

The first equation implies that either  $\lambda = 0$  or  $v_0 = 0$ . In both cases, the last equation implies that  $\mathbf{v} = 0$ .

We next introduce the infinite shift-down operator,

$$\mathbf{S} \equiv \begin{bmatrix} 0 & 0 & 0 & 0 & \cdots \\ 1 & 0 & 0 & 0 & \\ 0 & 1 & 0 & 0 & \\ 0 & 0 & 1 & 0 & \\ \vdots & & & & \ddots \end{bmatrix}. \quad (2.12)$$

This operator causes a vector to ‘‘slide down’’ and inserts a zero at the evacuated component at the top.  $\mathbf{S}$  has no eigenvectors at all, not even a fixed point (in spite of the fact that  $\sum_{i=0}^{\infty} S_{i,j} = 1$  for  $j = 0, \dots, \infty$ ). In fact,  $\mathbf{E}\mathbf{v} = p\mathbf{S}\mathbf{v}$  for all vectors  $\mathbf{v}$  with  $\sum_{j=0}^{\infty} v_j = 0$ .

Nevertheless, the convergence of  $\mathbf{P}(t)$  to  $\mathbf{P}^*$  is simple. Starting from any initial state vector  $\mathbf{P}(t=0)$ , the first application of  $\mathbf{E}$  causes the first component to be set to its steady-state value  $P_0(t=1) = q$ . At each subsequent iteration another component is set permanently:  $P_1(t=2) = qp$ ,  $P_2(t=3) = qp^2$ , etc.  $P_j$  becomes equal to  $P_j^*$  after no more than  $j+1$  time steps. The context we are interested in is wider. We wish to compute the convergence of ‘‘observables,’’ i.e., the average of an arbitrary function  $a(j)$ , over configurations. We compute the average at time  $t$ ,

$$\langle a \rangle(t) \equiv \sum_{j=0}^{\infty} a(j) P_j(t) = \langle a \rangle^* + \sum_{j=0}^{\infty} a(j) v_j(t), \quad (2.13)$$

where  $\langle a \rangle^* \equiv \sum_{j=0}^{\infty} a(j) P_j^*$  is the steady-state average. Starting from an initial deviation from the steady state  $\mathbf{v}(0)$ , each iteration causes a down shift and a multiplication by  $p$ , hence

$$\langle a \rangle(t) = \langle a \rangle^* + p^t \sum_{j=0}^{\infty} a(j+t) v_j(0). \quad (2.14)$$

Equation (2.14) is the analog of the standard eigenvector description. We can also identify here the exponential decay of the factor  $p^t$ . For example, the function  $a(j) = \delta_{j,j_0}$  ‘‘measures’’ the probability of the climber to be at height  $j_0$  (at any time). At time  $t$  the observed average probability is

$$\langle a \rangle(t) = P_{j_0}^* + p^t v_{j_0-t}(0), \quad (2.15)$$

for  $t \leq j_0$ , and  $\langle a \rangle(t) = P_{j_0}^*$  for  $t > j_0$  [16].

### A. First-order approximation for $N=2$

We now return to Eq. (1.13), and try to approximate it by a sequence of models which are related to the frustrated climber model. The simplest approximation would follow if we do not let the particle penetrate into the fjord at all. This is equivalent to setting  $\kappa_f = \infty$  in Eq. (1.13). According to these simplified rules, the particle can either stick at  $(0,0)$  and create a flat step of  $i=0$ , or it can stick at  $(1,1)$  and increase the step height by 1. Let us denote the probability

for the former event by  $q$  and the latter by  $p$ . In the first-order approximation we take  $p$  and  $q$  to be independent of the initial step size  $j$ , unless  $j=0$ , in which case the step size increases with probability 1. The Markovian matrix  $\mathbf{E}$  for this case is almost identical to the case of the frustrated climber,

$$\mathbf{E} = \begin{bmatrix} q_0 & q & q & q & \cdots \\ p_0 & 0 & 0 & 0 & \\ 0 & p & 0 & 0 & \\ 0 & 0 & p & 0 & \\ \vdots & & & & \ddots \end{bmatrix}, \quad (2.16)$$

the only difference being in the first column, where we denote  $q_0=0$  and  $p_0=1$ . In Ref. [12] we show that this model is exact for the case of site-sticking DLA for  $N=2$ .

The solution to this problem is very similar to that of the frustrated climber, with small modifications. The steady state is

$$P_j^* = P_0^* p_0 p^{j-1}, \quad j \geq 1, \quad (2.17)$$

where  $P_0^*$  can be determined using the normalization condition

$$1 = \sum_{j=0}^{\infty} P_j^* = P_0^* \left( 1 + p_0 \sum_{j=0}^{\infty} p^j \right), \quad (2.18)$$

$$\Rightarrow P_0^* = \frac{1-p}{1-p+p_0}.$$

The average upward growth probability is evaluated by

$$\langle p_{\text{up}}^{(1)} \rangle^* = P_0^* p_0 + (1 - P_0^*) p = \frac{p_0}{1-p+p_0}. \quad (2.19)$$

The superscript (1) appears because it is the first-order approximation. We now need to choose  $p$ . One possible choice would be to take  $p = E_{\infty+1, \infty} = 0.5658$ , because this is the asymptotic upward growth probability, and then set  $q = 1 - p$ . This would give  $\langle p_{\text{up}}^{(1)} \rangle^* = 0.6973$ , to be compared with the exact value 0.6812 [15]. An alternative approximation would return to Eq. (1.13), but replace  $y(\infty)$  by  $q$ , and then find  $q$  by solving  $1 = p + q = [1 + g_2(1)q]/2 + q$ . This yields  $p = 1 - q = 2 - \sqrt{2} = 0.5858$ , and therefore  $\langle p_{\text{up}}^{(1)} \rangle^* = \sqrt{2}/2 = 0.7071$ .

We next calculate the average density and the fractal dimensionality. Similar to the argument used by Turkevich and Scher [17], we consider a large number of growth processes  $n$  in the steady state. During this growth the aggregate would grow higher by  $h = \langle p_{\text{up}} \rangle^* n$ . The total volume covered by the new growth is  $hN^{d-1}$ , where  $d=2$  is the Euclidean dimension. Thus, for  $N=2$  and for our first approximation, the density is

$$\rho = \frac{n}{hN^{d-1}} = \frac{n}{\langle p_{\text{up}} \rangle^* n N^{d-1}} = \frac{1}{\langle p_{\text{up}} \rangle^* N^{d-1}} = 0.7171, \quad (2.20)$$

to be compared with the exact value  $\rho = 0.7340$ . Although our model does not really produce fractal structures (due to the narrow width of our space), we can make an estimate of the fractal dimension in the same way Pietronero *et al.* estimated it in Refs. [6,18]. For a self similar fractal structure, one expects that a change of scale by a factor  $N$  will change the average mass (number of occupied sites) of a  $N \times N$  cut by a factor  $N^D$ , where  $D$  is the fractal dimension. Assuming that the above procedure represents a coarse graining of the sites into  $N \times N$  cells, we conclude that asymptotically

$$\rho = N^{D-d}, \quad (2.21)$$

and this means that

$$D = d + \frac{\ln(\rho)}{\ln(N)} = 1 - \frac{\ln(\langle p_{\text{up}} \rangle^*)}{\ln(N)} = 1.5202. \quad (2.22)$$

In Sec. IV we suggest a modified estimate of the fractal dimension, allowing for corrections to the asymptotic form (2.21).

The study of the convergence to the steady state is again limited to the subspace of vectors  $\mathbf{v}$  with  $\sum_{j=0}^{\infty} v_j = 0$ . The dynamic equation for  $i=0$  is,

$$v_0(t+1) = q_0 v_0(t) + \sum_{j=1}^{\infty} q v_j(t) = (q_0 - q) v_0(t),$$

$$\Rightarrow v_0(t) = (q_0 - q)^t v_0(0). \quad (2.23)$$

Since  $q_0=0$ , the exponentiated prefactor is negative, and therefore  $v_0(t)$  is oscillating during its decay. After the first iteration  $v_1(1) = p_0 v_0(0)$ , regardless of its initial value. Afterwards it continues to follow  $v_0$ , i.e.,  $v_1(t) = p_0 (q_0 - q)^{t-1} v_0(0)$ . After the second iteration  $v_2(2) = p_0 p v_0(0)$ , and it also starts to decay exponentially with the factor  $(q_0 - q)$ . This happens for any  $j > 1$ ; after more than  $j$  time steps ( $t > j$ ) one has,

$$v_j(t) = p_0 p^{j-1} (q_0 - q)^{t-j} v_0(0). \quad (2.24)$$

For short times and large indices  $t < j$ , the dynamics is governed by the shift-down operator,

$$\mathbf{v}(t) = v_0(0) (q_0 - q)^t \mathbf{h} + p^t \sum_{j=1}^{\infty} c_j \mathbf{e}^{(j+t)}, \quad (2.25)$$

where  $\mathbf{e}^{(j)}$  are the standard basis vectors, the components of the vector  $\mathbf{h}$  are,

$$h_0 \equiv 1,$$

$$h_j \equiv \frac{p_0}{p} \left( \frac{p}{q_0 - q} \right)^j, \quad j \geq 1, \quad (2.26)$$

and the constants  $c_j$  are determined by the initial conditions,

$$c_j = v_j(0) - v_0(0) h_j, \quad j = 1, 2, \dots \quad (2.27)$$

For  $p > 0.5$  the components of  $\mathbf{h}$  explode exponentially. However,  $\sum_{j=0}^{\infty} v_j(0) = 0$  and therefore  $\lim_{j \rightarrow \infty} v_j(0) = 0$ . Thus, in order to cancel the divergence of the  $h_j$ 's, the  $c_j$ 's

must also explode exponentially and have an opposite sign. We note that because of this divergence  $\mathbf{h}$  does not have a finite  $L_1$  norm and thus does not belong to the domain of  $\mathbf{E}$ . Therefore it is not an eigenvector.

### B. Higher-order approximations for $N=2$

As mentioned earlier, the frustrated climber model resembles the bond-DLA evolution matrix (1.13), (1.15). In this section we approximate the full dynamics using increasingly more complex matrices. By doing so we do not improve on the accuracy of our previously published results [15], but rather learn about the rate of convergence to the steady state. The method used in this section is generalized and applied to cylindrical DLA with wider periods in the next section. The case  $N=2$  is the simplest demonstration of this approach.

The second-order approximation is to allow also transitions of the kind  $j \rightarrow 1$  for  $j \geq 1$ . We also allow having arbitrary values in the top left  $2 \times 2$  corner of the matrix, which we copy from the original matrix of Eq. (1.15), i.e.,

$$\mathbf{E} = \begin{bmatrix} q_0 & q_1 & q & q & q & \cdots \\ r_0 & r_1 & r & r & r & \\ 0 & p_1 & 0 & 0 & 0 & \\ 0 & 0 & p & 0 & 0 & \\ 0 & 0 & 0 & p & 0 & \\ \vdots & & & & & \ddots \end{bmatrix}. \quad (2.28)$$

We still require that the sum of the elements in each column be equal to 1, i.e.,

$$\begin{aligned} q_0 + r_0 &= 1, \\ q_1 + r_1 + p_1 &= 1, \\ q + r + p &= 1. \end{aligned} \quad (2.29)$$

In terms of standard DLA this means that we allow the particle to penetrate two sites into the fjord, but no more. Indeed it is exponentially improbable to penetrate deep into the fjord. This fact suggests a controlled approximation for DLA. In each order of the approximation we allow the depth of penetration into the fjord to grow by 1. This is done by copying the  $(O+1) \times O$  upper left block of the original matrix (1.13), (1.15), where  $O$  is the order of approximation. Asymptotic values are used outside this block, i.e.,

$$\begin{aligned} E_{j+1,j} &= E_{\infty+1,\infty}, \quad j \geq O, \\ E_{i,j} &= y(\infty)e^{-\kappa_f i}, \quad j \geq O, \quad i \leq O-2, \\ E_{n-1,j} &= 1 - \sum_{i=0}^{n-2} y(\infty)e^{-\kappa_f i} - E_{\infty+1,\infty} = y(\infty) \frac{e^{-\kappa_f(n-1)}}{1 - e^{-\kappa_f}}, \\ & \quad j \geq O, \end{aligned} \quad (2.30)$$

and the rest of the matrix elements are null. For example, in our case,  $O=2$ , the constants in the matrix (2.28) are

$$q_0 = 0,$$

$$r_0 = 1,$$

$$q_1 = \frac{6 - 3\sqrt{2}}{4} = 0.4393,$$

$$r_1 = 0,$$

$$p_1 = \frac{3\sqrt{2} - 2}{4} = 0.5607,$$

$$q = y(\infty) = \sqrt{3} - \sqrt{2} = 0.3178,$$

$$p = E_{\infty+1,\infty} = 0.5658,$$

$$r = y(\infty) \frac{e^{-\kappa_f}}{1 - e^{-\kappa_f}} = 0.1163.$$

First, the steady state is found by solving  $\mathbf{P}^* = \mathbf{E}\mathbf{P}^*$ , i.e.,

$$\begin{aligned} P_0^* &= q_0 P_0^* + q_1 P_1^* + q \sum_{j=2}^{\infty} P_j^*, \\ P_1^* &= q_0 P_0^* + q_1 P_1^* + r \sum_{j=2}^{\infty} P_j^*, \\ P_2^* &= p_1 P_1^*, \\ P_{j+1}^* &= p P_j^*, \quad j \geq 2. \end{aligned} \quad (2.32)$$

The solution to the last equation is

$$P_j^* = P_2^* p^{j-2}, \quad j \geq 2. \quad (2.33)$$

Keeping this in mind it is possible to exchange the two last equations of the set (2.32) with

$$\sum_{j=2}^{\infty} P_j^* = p_1 P_1^* + p \sum_{j=2}^{\infty} P_j^*. \quad (2.34)$$

Thus we obtain an autonomous and finite set of three equations for three unknowns, namely,  $P_0^*$ ,  $P_1^*$  and  $\tilde{P}_2^* \equiv \sum_{j=2}^{\infty} P_j^*$ . The third parameter,  $\tilde{P}_2^*$ , represents the total probability for the infinitely many configurations with  $j \geq 2$ . This reduction of the problem to three parameters became possible because all of the configurations with  $j \geq 2$  have exactly the same transition probabilities to the configurations  $j=0$  and  $j=1$ , and because they have exactly the same upward growth probability. Thus we obtain a fixed point equation for a three-component vector,

$$\begin{bmatrix} P_0^* \\ P_1^* \\ \tilde{P}_2^* \end{bmatrix} = \begin{bmatrix} q_0 & q_1 & q \\ r_0 & r_1 & r \\ 0 & p_1 & p \end{bmatrix} \begin{bmatrix} P_0^* \\ P_1^* \\ \tilde{P}_2^* \end{bmatrix}. \quad (2.35)$$

It is guaranteed that a nontrivial solution exists, because the sum of the terms in each column of the finite matrix equals 1. Using the constants from Eqs. (2.31), the normalized solution obtained is,

TABLE II. Some steady-state results of the third-order approximation.

	$\langle p_{\text{up}} \rangle^*$	$P_0^*$	$P_1^*$	$P_2^*$	$P_3^*$	$P_4^*$	$P_5^*$
Third order	0.6812	0.2696	0.3114	0.1820	0.1029	0.0582	0.0329
Accurate	0.6812	0.2696	0.3113	0.1809	0.1032	0.0586	0.0332

$$\begin{aligned}
P_0^{*(2)} &= 0.2705, & (0.2696), \\
P_1^{*(2)} &= 0.3184, & (0.3113), \\
\tilde{P}_2^{*(2)} &= 0.4111, & (0.4191),
\end{aligned} \tag{2.36}$$

where the superscript denotes the order of approximation and a comparison is drawn to the exact values in parentheses. By ‘‘exact’’ we refer to very high order calculations, or to values from simulations (which are the same up to the presented accuracy of  $10^{-4}$ ) [15]. The elements  $P_j^*$  for  $j \geq 2$  are evaluated using

$$P_j^{*(2)} = (1-p)\tilde{P}_2^{*(2)}p^{j-2}, \quad j \geq 2. \tag{2.37}$$

It is now possible to evaluate the average upward growth probability

$$\langle p_{\text{up}}^{(2)} \rangle^* = P_0^* r_0 + P_1^* p_1 + \tilde{P}_2^* p = 0.6816, \tag{2.38}$$

where the exact value is 0.6812. The fractal dimension is evaluated as in Eq. (2.22),

$$D^{(2)} = 1.5530, \tag{2.39}$$

compared to the exact value 1.5538.

The temporal convergence to the steady state in the second-order approximation can be analyzed using both the shift-down operator and eigenvectors. The first eigenvector of the matrix in Eq. (2.35) is the fixed point solution, which we denote by  $\tilde{\mathbf{P}}^*$ . Let us denote the other two (three-components) eigenvectors by  $\tilde{\mathbf{h}}$  and  $\tilde{\mathbf{g}}$ , and their corresponding eigenvalues by  $|\lambda_0| \geq |\lambda_1|$ . After  $t$  iterations of the evolution matrix we have

$$\tilde{\mathbf{P}}(t) = \tilde{\mathbf{P}}^* + c_0 \lambda_0^t \tilde{\mathbf{h}} + c_1 \lambda_1^t \tilde{\mathbf{g}}, \tag{2.40}$$

where  $c_0$  and  $c_1$  are constants determined by the initial conditions. The configurational average of some function  $a(j)$  with  $a(j) = a(2)$  for  $j > 2$ , can be expressed in terms of these eigenvalues only,

$$\langle a \rangle(t) = \langle a \rangle^* + k_0 \lambda_0^t + k_1 \lambda_1^t, \tag{2.41}$$

where  $k_0$  and  $k_1$  are some other constants. A special function of this type is the upward growth probability,  $p_{\text{up}}(j) = (r_0, p_1, p, p, p, \dots)$ . The eigenvalue with the largest absolute value other than 1,  $\lambda_0$ , makes the largest contribution to the deviation from the steady-state values, and thus controls the temporal convergence. The characteristic time constant for the exponential convergence is,

$$\tau = -\frac{1}{\ln(|\lambda_0|)}. \tag{2.42}$$

The eigenvalues obtained are  $\lambda_0^{(2)} = -0.5599$  and  $\lambda_1^{(2)} = 0.1257$ , using the constants of Eqs. (2.31). Hence,  $\tau^{(2)} = 1.7$ . In order to describe the convergence of  $P_j(t)$  for  $j \geq 2$  we use the vector  $\mathbf{v}(t) = \mathbf{P}(t) - \mathbf{P}^*$ , once more, and we perform a decomposition similar to Eq. (2.25),

$$\mathbf{v}(t) = c_0 \lambda_0^t \mathbf{h} + c_1 \lambda_1^t \mathbf{g} + p^t \sum_{j=2}^{\infty} c_j \mathbf{e}^{(j+t)}, \tag{2.43}$$

where  $c_0$  and  $c_1$  are the same as in Eq. (2.40) and the constants  $c_j$  for  $j \geq 2$  are determined by the initial condition  $\mathbf{v}(0)$ . The vectors  $\mathbf{h}$  and  $\mathbf{g}$  are infinite generalizations of the finite vectors  $\tilde{\mathbf{h}}$  and  $\tilde{\mathbf{g}}$ , according to

$$\begin{aligned}
h_j &= \tilde{h}_j, & g_j &= \tilde{g}_j, & j &= 0, 1, \\
h_2 &= p_1 \tilde{h}_1, & g_2 &= p_1 \tilde{g}_1, & j &= 2, \\
h_j &= h_2 \left( \frac{p}{\lambda_0} \right)^{j-2}, & g_j &= g_2 \left( \frac{p}{\lambda_1} \right)^{j-2}, & j &\geq 2.
\end{aligned} \tag{2.44}$$

Because  $p = E_{\infty+1, \infty} > |\lambda_0|, |\lambda_1|$ , it is apparent that the components  $h_j$  and  $g_j$  diverge exponentially for large  $j$ 's. This means that these vectors do not have a finite  $L_1$  norm, and that they do not belong to the domain of  $\mathbf{E}$ . Therefore, they are not eigenvectors, and  $\lambda_0$  and  $\lambda_1$  are not eigenvalues of  $\mathbf{E}$ . Nevertheless, Eq. (2.43) is still true. The effect of the shift-down operator is manifested in the sum  $p^t \sum_{j=2}^{\infty} c_j \mathbf{e}^{(j+t)}$ .

Using the same method it is possible to make higher-order calculations. The steady-state quantities resulting from the third-order approximation are presented in Table II, in comparison with exact results. The eigenvalue with the largest absolute value is  $\lambda_0^{(3)} = -0.5687$ , which has a greater absolute value than  $E_{\infty+1, \infty} = 0.5658$ . This means that a legitimate eigenvector exists for the infinite matrix. In the fourth- and fifth-order approximation we get  $\lambda_0^{(4,5)} \approx -0.5688$ . This suggests that the higher the order the more accurate is the evaluation of  $\lambda_0$  and that the accuracy obtained is better than  $10^{-4}$ . The typical time needed to settle in the steady state from any initial condition is therefore as short as

$$\tau = 1.8. \tag{2.45}$$

### III. DLA WITH $N > 2$

The generalization of the exact methods from Ref. [15] to  $N > 2$  is not straightforward. Trying to proceed along a similar line, one would try to parametrize the interface with a parameter  $i = 1, 2, \dots, \infty$ , and write the Master equation  $P_i(t+1) = \sum_{j=1}^{\infty} E_{i,j} P_j(t)$ . Unlike the case  $N=2$ , the parameterization for  $N > 2$  is very complicated. For instance, for the case  $N=3$  it is reasonable to try using two parameters, which indicate the height of two columns relative to the



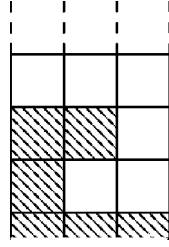


FIG. 3. An example of an interface configuration for  $N=3$  that cannot be characterized using the height differences of two columns relative to the third.

highest (or lowest) third column. However, this is insufficient because complex fjords (involving overhangs) might occur, as shown in Fig. 3. Instead of achieving a perfect parametrization, we adopt the approximate approach of Sec. II B, i.e., we take into account only a finite number of interface configurations. These configurations are classified according to the maximum height difference between the highest and lowest particles on the interface  $\Delta m$ . In the  $O$ th-order approximation all the configurations with  $\Delta m \leq O$  are included. The excluded configurations with  $\Delta m > O$  are transformed into a configuration with  $\Delta m = O$ , by filling in the  $(O+1)$ th row below the highest particle; see Fig. 4. This transformation does not change the growth probabilities considerably. Especially, the upward growth probability would hardly change for large  $O$ . The variable  $P_i(t)$ , where  $i$  corresponds to a configuration with  $\Delta m = O$ , actually represents the sum of probabilities of all the configurations with  $\Delta m \geq O$ , that have the same  $O$  uppermost rows, rather than represent the probability of the configuration  $i$  alone. This is analogous to  $\tilde{P}_2^*$  in the example above, see Sec. II B. After the finite set of configurations is chosen, the configurations are indexed with arbitrary consecutive numbers. Then, the growth probabilities for each configuration are computed by solving the Laplace equation and by taking into account the bond multiplicity. Each growth process results in a different final configuration, which must be identified with one of the configurations in the finite set. Special attention is required for the upward growth processes, which might result in configurations with  $\Delta m > O$ , which do not belong to the finite set. This is rectified by truncating the bottom row of the interface (considering it as fully occupied). The total upward probability for each configuration is added up and stored in a function  $p_{\text{up}}(i)$ , later to be averaged over the steady-state distribution of configurations. The growth probabilities are arranged in the evolution matrix,  $\mathbf{E}$ , whose fixed point corresponds to the steady-state distribution of configurations, which is required for evaluating  $\langle p_{\text{up}} \rangle^*$ ,  $\rho$  and  $D$ . Because the matrix is finite, the existence of at least one

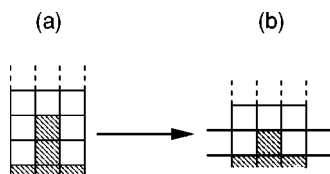


FIG. 4. Configuration (a), with  $\Delta m = 2$ , is truncated by taking only the top row, and turns into configuration (b), with  $\Delta m = 1$ , in the first-order approximation ( $O = 1$ ).

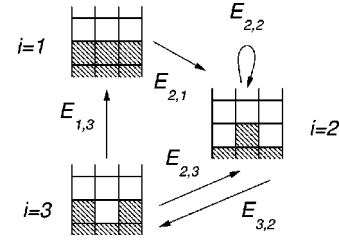


FIG. 5. The three possible configurations in the first-order approximation for  $N=3$ , up to translation symmetry. The arrows indicate the possible transitions due to growth processes. The transition probability from configuration  $j$  to  $i$  is denoted by  $E_{i,j}$ .

fixed point is guaranteed. The other eigenvectors describe the rate of convergence to the steady state.

The best way to demonstrate this approach is by showing a few sample calculations. The easiest ones are the first- and second-order approximation for  $N=3$  and the first-order approximation for  $N=4$ . After that we explain the general algorithm for higher orders and widths, and report the results obtained numerically.

#### A. First-order approximation for $N=3$

In the first-order approximation we only look at the top row of the aggregate. For  $N=3$  there are only three possible configurations (up to symmetry), with the top row occupied by 1, 2 or 3 particles. Each configuration is indexed and for each configuration we identify the growth processes and the final configurations resulting from them; see Fig. 5. In Ref. [12] we show that the calculation presented in this section can be used to solve exactly (no approximations) the case of site-DLA with  $N=3$ .

The first configuration ( $j=1$ ) grows upward with probability 1, thus  $p_{\text{up}}(1)=1$ . The resulting configuration is  $i=2$ , thus  $E_{2,1}=1$  and  $E_{i,1}=0$  for  $i \neq 2$ . This concludes the construction of the first column of the evolution matrix.

In order to obtain the other growth probabilities we have to solve the relevant Laplace problems, for which we need the Green's function according to Eq. (1.11). For  $N=3$  we have  $k_l = (2\pi/3)l$  for  $l=0,1,2$ . We recall that  $e^{-\kappa(k)} = q - \sqrt{q^2 - 1}$ , where  $q = 2 - \cos(k)$  [15] and find that

$$\begin{aligned} e^{-\kappa_0} &= 1, \\ e^{-\kappa_1} &= e^{-\kappa_2} = \frac{5 - \sqrt{21}}{2}, \end{aligned} \quad (3.1)$$

and thus

$$\begin{aligned} g_3(0) &= \frac{1}{3} \left( 1 + 2 \frac{5 - \sqrt{21}}{2} \right) = \frac{6 - \sqrt{21}}{3}, \\ g_3(1) &= g_3(2) = \frac{1 - g_3(0)}{2} = \frac{\sqrt{21} - 3}{6}. \end{aligned} \quad (3.2)$$

These values obey the normalization condition (1.12).

Because of the symmetry of the configuration  $j=2$ , the potential can be expressed in terms of one variable  $x \equiv \Phi(0,0) = \Phi(0,2)$ , as shown in Fig. 6. This kind of figure demonstrates the distribution of the potential  $\Phi(m,n)$  over

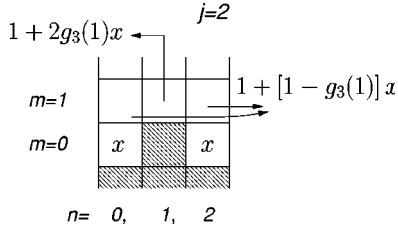


FIG. 6. A ‘‘potential diagram:’’ the potentials  $\Phi(m,n)$  of the configuration  $j=2$ , expressed in terms of the variable  $x$ .

the lattice, and thus we call it a ‘‘potential diagram.’’ The potentials  $\Phi(1,0)=\Phi(1,2)=1+(1-g_3(1))x$  do not correspond to a growth process, but are important for solving for  $x$ . The potential  $\Phi(1,1)=1+2xg_3(1)$  corresponds to the upward growth process. The Laplace equation for  $x$  is

$$4x = x + (1 - g_3(1))x + 1, \\ \Rightarrow x = \frac{9 - \sqrt{21}}{10} = 0.4417. \quad (3.3)$$

Growth in both sites  $(0,0)$  and  $(0,2)$  results in configuration  $i=3$ , hence

$$E_{3,2} = \frac{4}{3}x = \frac{18 - 2\sqrt{21}}{15} = 0.5890, \quad (3.4)$$

where the numerator, 4, is inserted because there are two bonds for each of the two growth sites, and the denominator is the normalization factor  $N=3$ . A growth process in site  $(1,1)$  results in an interface that does not belong to our finite set. In this approximation we only take into account the top-most row of the interface, and therefore this interface is identified with configuration  $i=2$ , i.e.,

$$E_{2,2} = \frac{2xg_3(1) + 1}{3} = \frac{2\sqrt{21} - 3}{15} = 0.4110. \quad (3.5)$$

The transition to  $i=1$  is impossible, hence,  $E_{1,2}=0$ . It is easy to check that the second column of the matrix is normalized, i.e.,  $\sum_{i=1}^3 E_{i,2}=1$ . The total upward growth probability for this configuration is

$$p_{\text{up}}(2) = E_{2,2} = 0.4110. \quad (3.6)$$

The potentials of configuration  $j=3$  are described in terms of  $x = \Phi(0,1)$ , as in Fig. 7. The Laplace equation is

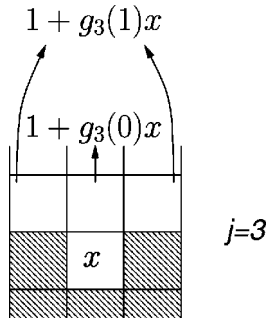


FIG. 7. The ‘‘potential diagram’’ for configuration  $j=3$ .

$$4x = g_3(0)x + 1, \\ \Rightarrow x = \frac{6 - \sqrt{21}}{5} = 0.2835. \quad (3.7)$$

There are three bonds leading to growth in site  $(1,0)$ , which results in the configuration  $i=1$ , hence

$$E_{1,3} = \frac{3}{3}x = 0.2835. \quad (3.8)$$

The upward growth process results in  $i=2$  after truncation, and has probability

$$p_{\text{up}}(3) = E_{2,3} = \frac{2}{3}(1 + g_3(1)x) = 0.7165. \quad (3.9)$$

The third element in the column is  $E_{3,3}=0$ , which concludes the calculation of the elements of the evolution matrix,

$$\mathbf{E}^{(3,1)} = \begin{bmatrix} 0 & 0 & 0.2835 \\ 1 & 0.4110 & 0.7165 \\ 0 & 0.5890 & 0 \end{bmatrix}, \quad (3.10)$$

where the superscript indicates that it is the first-order approximation for  $N=3$ . The upward growth probabilities series is

$$p_{\text{up}} = (1, 0.4110, 0.7165), \quad (3.11)$$

which happens to be equal to the second row of the matrix.

The normalized fixed point of the matrix is  $P_1^* = 0.0951$ ,  $P_2^* = 0.5695$  and  $P_3^* = 0.3354$ . The average upward growth probability is

$$\langle p_{\text{up}} \rangle^* = \sum_{i=1}^3 P_i^* p_{\text{up}}(i) = 0.5695. \quad (3.12)$$

We have performed some DLA simulations in the cylindrical geometry for several values of  $N$  and measured  $\langle p_{\text{up}} \rangle^*$  [19]. The value obtained from simulations for  $N=3$  is 0.5462. The typical accuracy is on the order of  $10^{-4}$ . The steady-state average density and fractal dimension are evaluated using Eqs. (2.20) and (2.22),

$$\rho = \frac{1}{3\langle p_{\text{up}} \rangle^*} = 0.5853, \quad (0.6103), \\ D = 1 - \frac{\ln(\langle p_{\text{up}} \rangle^*)}{\ln(3)} = 1.5125, \quad (1.5506). \quad (3.13)$$

The values in parentheses are obtained from the same formulas, using the simulation value of  $\langle p_{\text{up}} \rangle^*$ . The two other eigenvalues are complex,  $\lambda_{0,1} = -0.29 \pm 0.28i$ , so according to Eq. (2.42)  $\tau = 1.10$ .

## B. Higher-order approximations for $N=3$

The possible configurations of the interface in the second-order approximation are listed and indexed in Fig. 8. The growth probabilities for the first three configurations were

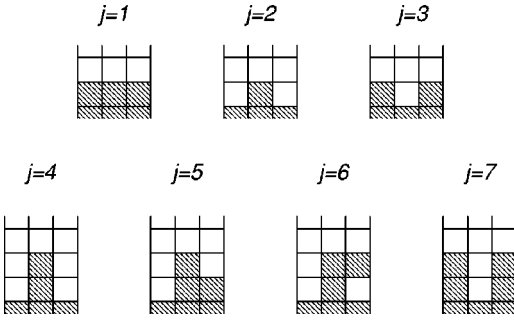


FIG. 8. Possible configurations in the second-order approximation for  $N=3$ . Note that the first three configurations,  $j=1,2,3$ , are the same as in the first-order approximation.

already computed in the previous section, but a rearrangement of the upward growths is required in the evolution matrix. Now, the upward growth from configuration  $j=2$  no longer stays at  $i=2$ , but rather makes a transition to  $i=4$ , and the upward growth from  $j=3$  results in  $i=5$  instead of  $i=2$ . Thus, we copy the previous evolution matrix  $\mathbf{E}^{(3,1)}$  into the upper left corner of the new matrix  $\mathbf{E}^{(3,2)}$  with the replacements:  $E_{2,2}^{(3,2)}=0$ ,  $E_{4,2}^{(3,2)}=E_{2,2}^{(3,1)}$ ,  $E_{2,3}^{(3,2)}=0$ , and  $E_{5,3}^{(3,2)}=E_{2,3}^{(3,1)}$ . The unspecified elements in the first three columns are all equal to zero.

The next step is to go over each of the remaining configurations  $i=4, \dots, 7$ , and compute their probabilities, which are inserted into the evolution matrix according to the final configuration in which the relevant growth process results. Configuration 4 is shown in Fig. 9. The Laplace equation is

$$\begin{aligned} 4y &= y + x, \\ 4x &= x + y + 1 + (1 - g_3(1))x, \\ \Rightarrow x &= \frac{3}{14}(7 - \sqrt{21}) = 0.5180, \\ y &= x/3 = 0.1727. \end{aligned} \tag{3.14}$$

The growth probabilities are

$$\begin{aligned} E_{6,4} &= \frac{2}{3}x = 0.3453, \\ E_{5,4} &= \frac{4}{3}y = \frac{4}{9}x = 0.2302, \\ E_{4,4} &= \frac{1 + 2xg_3(1)}{3} = 0.4244. \end{aligned} \tag{3.15}$$

The upward growth probability is  $p_{\text{up}}(4) = E_{4,4} = 0.4244$ .

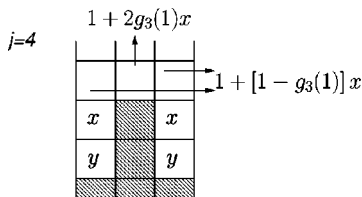


FIG. 9. The ‘potential diagram’ for configuration  $j=4$ .

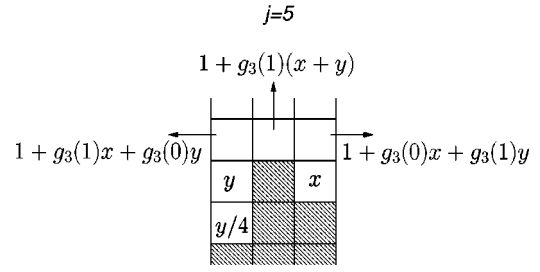


FIG. 10. The ‘potential diagram’ for configuration  $j=5$ .

Configuration 5 is shown in Fig. 10. The Laplace equations are

$$\begin{aligned} 4y &= y/4 + x + xg_3(1) + yg_3(0) + 1, \\ 4x &= y + g_3(0)x + g_3(1)y + 1, \\ \Downarrow \\ y &= 0.4808, \\ x &= 0.4557. \end{aligned} \tag{3.16}$$

The growth probabilities are

$$\begin{aligned} E_{7,5} &= \frac{2}{3}x = 0.3038, \\ E_{3,5} &= \frac{y}{3} = 0.1603, \\ E_{2,5} &= \frac{3}{3}y/4 = 0.1202, \\ E_{4,5} &= \frac{1 + g_3(1)(x + y)}{3} = 0.4157. \end{aligned} \tag{3.17}$$

The upward growth probability is  $p_{\text{up}}(5) = E_{4,5} = 0.4157$ .

Configuration 6 is shown in Fig. 11. The Laplace equations are

$$\begin{aligned} 4y &= y/4 + x, \\ 4x &= y + g_3(0)x + 1, \\ \Downarrow \\ x &= \frac{15}{151}(26 - 5\sqrt{21}) = 0.3067, \\ y &= \frac{4}{15}x = 0.0818. \end{aligned} \tag{3.18}$$

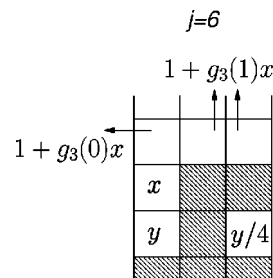


FIG. 11. The ‘potential diagram’ for configuration  $j=6$ .

The growth probabilities are

$$\begin{aligned}
 E_{1,6} &= \frac{2}{3}x = 0.2044, \\
 E_{3,6} &= \frac{2}{3}y = \frac{8}{45}x = 0.0545, \\
 E_{7,6} &= \frac{3}{3}y/4 = x/15 = 0.0204, \\
 E_{5,6} &= \frac{2}{3}(1 + g_3(1)x) = 0.7206.
 \end{aligned}
 \tag{3.19}$$

The upward growth probability is  $p_{\text{up}}(6) = E_{5,6} = 0.7206$ .

Configuration 7 is shown in Fig. 12. The Laplace equations are

$$\begin{aligned}
 4x &= x/4 + g_3(0)x + 1, \\
 \Downarrow \\
 x &= \frac{12}{105}(21 - 4\sqrt{21}) = 0.3051.
 \end{aligned}
 \tag{3.20}$$

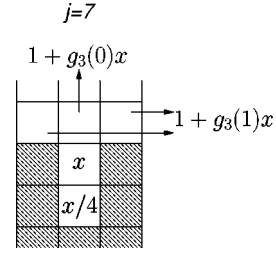


FIG. 12. The ‘‘potential diagram’’ for configuration  $j=7$ .

The growth probabilities are

$$\begin{aligned}
 E_{1,7} &= \frac{2}{3}x = 0.2304, \\
 E_{3,7} &= \frac{3}{3}x/4 = 0.0763,
 \end{aligned}
 \tag{3.21}$$

$$E_{5,7} = \frac{2}{3}(1 + g_3(1)x) = 0.7203.$$

The upward growth probability is  $p_{\text{up}}(7) = E_{5,7} = 0.7203$ .

In summary,

$$\mathbf{E}^{(3,2)} = \begin{bmatrix} 0 & 0 & 0.2835 & 0 & 0 & 0.2044 & 0.2034 \\ 1 & 0 & 0 & 0 & 0.1202 & 0 & 0 \\ 0 & 0.5890 & 0 & 0 & 0.1603 & 0.0545 & 0.0763 \\ 0 & 0.4110 & 0 & 0.4244 & 0.4157 & 0 & 0 \\ 0 & 0 & 0.7165 & 0.2302 & 0 & 0.7206 & 0.7203 \\ 0 & 0 & 0 & 0.3453 & 0 & 0 & 0 \\ 0 & 0 & 0 & 0 & 0.3038 & 0.0204 & 0 \end{bmatrix},
 \tag{3.22}$$

$$p_{\text{up}} = (1, 0.4110, 0.7165, 0.4244, 0.4157, 0.7206, 0.7203).
 \tag{3.23}$$

One can check that elements in each column of the matrix sum up to 1. Note that the majority of the elements are null. The normalized fixed point is,

$$\mathbf{P}^* = (0.0685, 0.1011, 0.1145, 0.2680, 0.2711, 0.0925, 0.0843),
 \tag{3.24}$$

with which we compute some steady-state quantities,

$$\langle p_{\text{up}} \rangle^* = \sum_{j=1}^7 P_j^* p_{\text{up}}(j) = 0.5459, \quad (0.5462),$$

$$\rho = \frac{1}{3\langle p_{\text{up}} \rangle^*} = 0.6106, \quad (0.6103),
 \tag{3.25}$$

$$D = 1 - \frac{\ln(\langle p_{\text{up}} \rangle^*)}{\ln(3)} = 1.5510, \quad (1.5506),$$

where once again, the values from simulation are shown in parentheses. It is apparent that the addition of configurations increases the accuracy of the results. The eigenvalues with the largest absolute values (except for 1) are  $\lambda_{0,1} = -0.34 \pm 0.40i$ , hence  $\tau = 1.6$ .

The third-order approximation yields 17 configurations. The final results are

$$\langle p_{\text{up}} \rangle^* = \sum_{j=1}^{17} P_j^* p_{\text{up}}(j) = 0.5460, \quad (0.5462),$$

$$\rho = \frac{1}{3\langle p_{\text{up}} \rangle^*} = 0.6104, \quad (0.6103),
 \tag{3.26}$$

$$D = 1 - \frac{\ln(\langle p_{\text{up}} \rangle^*)}{\ln(3)} = 1.5507, \quad (1.5506).$$

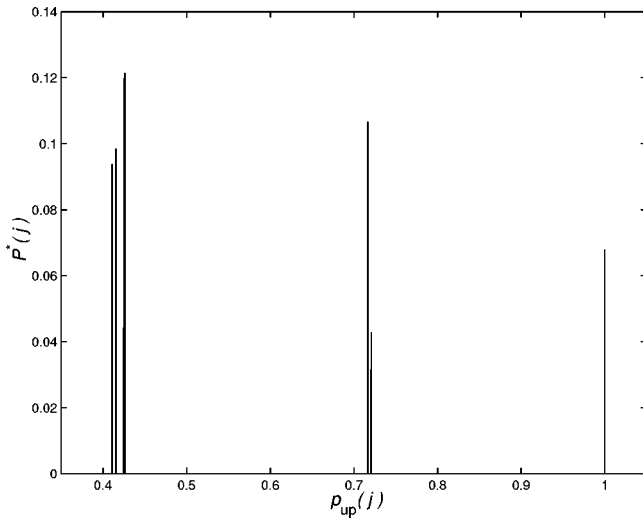


FIG. 13. The distribution of  $p_{\text{up}}$  over configurations for the third-order approximation for  $N=3$ .

The eigenvalues with the largest absolute values (except for 1) are  $\lambda_{0,1} = -0.34 \pm 0.40i$ , hence  $\tau = 1.6$ .

It is interesting to inspect the histogram of the distribution of  $p_{\text{up}}(j)$ , illustrated in Fig. 13. One immediately observes that the upward growth probabilities are clustered in three groups: the top one at 1, the second just above 0.7 and the third, just above 0.4. It is easy to check that the top one corresponds to the configuration  $i=1$ , the middle group corresponds to configurations that have two particles at the top row, and the bottom group corresponds to configurations with one particle at the top row. This suggests that perhaps 17 different configurations are excessive, and the real number of effective configurations is around 3. An interesting question is whether it is possible to further reduce the number of configurations in higher-order approximations by including only ‘‘effective’’ ones.

**C. First-order approximation for  $N=4$**

Our last example is the case  $N=4$ , for which we present the first-order calculation. First, we calculate the Green’s function  $g_4(n)$  according to Eq. (1.11). For  $N=4$ , there are four possible values for  $k$  and  $\kappa$ , namely,  $k_l = (2\pi/N)l = 0, \pi/2, \pi, (3/2)\pi$ ,  $e^{-\kappa_0} = 1$ ,  $e^{-\kappa_1} = e^{-\kappa_3} = 2 - \sqrt{3}$ , and  $e^{-\kappa_2} = 3 - \sqrt{8}$ . Hence,

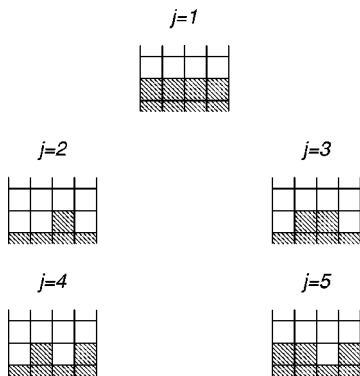


FIG. 14. Possible configurations in the first-order approximation for  $N=4$ .

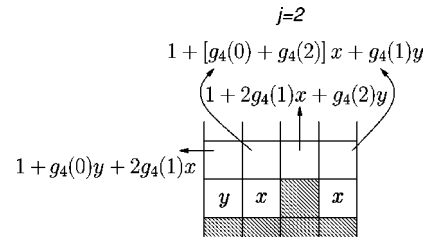


FIG. 15. The ‘‘potential diagram’’ for configuration  $j=2$ .

$$g_4(0) = \frac{1 + 2(2 - \sqrt{3}) + 3 - \sqrt{8}}{4} = 2 - \frac{\sqrt{3} + \sqrt{2}}{2} = 0.4269,$$

$$g_4(1) = g_4(3) = \frac{1 - 3 + \sqrt{8}}{4} = \frac{\sqrt{2} - 1}{2} = 0.2071, \quad (3.27)$$

$$g_4(2) = \frac{1 - 2(2 - \sqrt{3}) + 3 - \sqrt{8}}{4} = \frac{\sqrt{3} - \sqrt{2}}{2} = 0.1589.$$

Once again, Eq. (1.12) is obeyed.

Figure 14 displays the relevant configurations. Configuration  $j=1$  grows into configuration  $i=2$  with probability 1, thus  $E_{2,1} = 1$  and  $E_{i,1} = 0$  for  $i \neq 2$ . Also,  $p_{\text{up}}(1) = 1$ .

Configuration  $j=2$  is shown in Fig. 15. The Laplace equations are

$$\begin{aligned} 4x &= y + g_4(1)y + (g_4(0) + g_4(2))x + 1, \\ 4y &= 2x + g_4(0)y + 2g_4(1)x + 1, \end{aligned} \quad (3.28)$$

$$x = 0.5148,$$

$$y = 0.6277.$$

The nonzero growth probabilities in the second column are  $E_{3,2} = (4/3)x = 0.5148$ ,  $E_{4,2} = (1/4)y = 0.1569$ , and  $E_{2,2} = (1/4)(1 + 2g_4(1)x + g_4(2)y) = 0.3283 = p_{\text{up}}(2)$ .

Configuration  $j=3$  is presented in Fig. 16. The Laplace equation is

$$\begin{aligned} 4x &= x + (g_4(0) + g_4(1))x + 1, \\ \Rightarrow x &= 0.4226. \end{aligned} \quad (3.29)$$

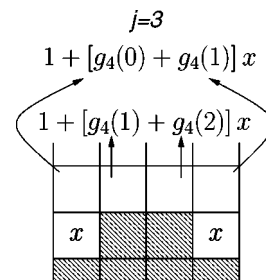
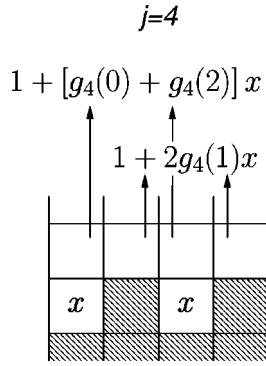


FIG. 16. The ‘‘potential diagram’’ for configuration  $j=3$ .

FIG. 17. The ‘‘potential diagram’’ for configuration  $j=4$ .

The nonzero growth probabilities in the third column are  $E_{5,3}=(4/4)x=0.4226$  and  $E_{2,3}=(2/4)[1+(g_4(1)+g_4(2))x]=0.5774=p_{\text{up}}(3)$ .

Configuration  $j=4$  is shown in Fig. 17. The Laplace equation is

$$4x=(g_4(0)+g_4(2))x+1, \quad (3.30)$$

$$\Rightarrow x=0.2929.$$

The nonzero growth probabilities in the fourth column are  $E_{5,4}=(6/4)x=0.4393$  and  $E_{2,4}=(2/4)(1+2g_4(1)x)=0.5607=p_{\text{up}}(4)$ . Note that this configuration already appeared for  $N=2$ .

The last configuration is shown in Fig. 18. The Laplace equation is

$$4x=1=g_4(0)x, \quad (3.31)$$

$$\Rightarrow x=0.2799.$$

The nonzero growth probabilities in the fifth column are  $E_{1,5}=(3/4)x=0.2099$  and  $E_{2,5}=(1/4)[3+(g_4(2)+2g_4(1))x]=0.7901=p_{\text{up}}(5)$ . This concludes the calculation of the  $5 \times 5$  evolution matrix  $\mathbf{E}^{(4,1)}$ .

The steady-state vector is

$$\mathbf{P}^*=(0.0298,0.4954,0.2551,0.0777,0.1420). \quad (3.32)$$

It enables us to calculate the following steady-state quantities:

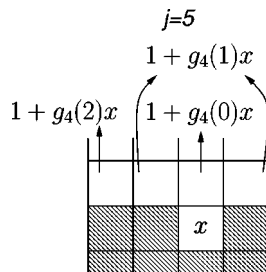
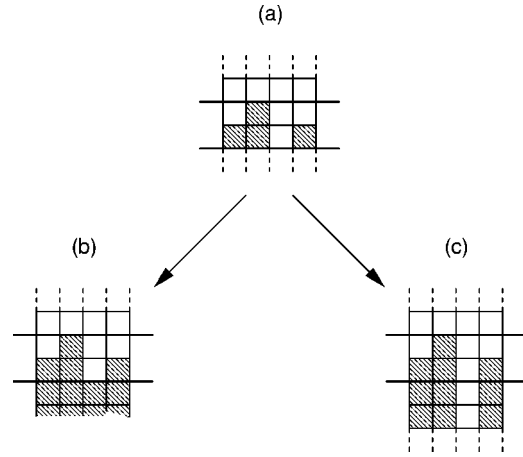
FIG. 18. The ‘‘potential diagram’’ for configuration  $j=5$ .

FIG. 19. The two top rows of a configuration are shown in (a). Two possible extensions for the rest of the configuration below are (b), with a filled row right below the configuration (this boundary condition is used in the calculations presented in this paper), or (c), with the bottom row of the configuration repeating itself *ad infinitum*, creating an infinite fjord.

$$\langle p_{\text{up}} \rangle^* = P_2^* = 0.4954, \quad (0.4657),$$

$$\rho = \frac{1}{4\langle p_{\text{up}} \rangle^*} = 0.5046, \quad (0.5368), \quad (3.33)$$

$$D = 1 - \frac{\ln(\langle p_{\text{up}} \rangle^*)}{\ln(4)} = 1.5066, \quad (1.5512),$$

where again, the values in parentheses are from simulation. The eigenvalues with the largest absolute value after 1 are  $\lambda_{0,1} = -0.16 \pm 0.38i$ , hence  $\tau = 1.1$ .

It is also possible to conduct these calculations using different boundary conditions at the bottom; rather than assuming that there is a filled row of occupied sites below the configuration, it is possible to assume that each unoccupied site at the lowest row of the configuration is above an infinite fjord that extends all the way below. The two possibilities are explained in Fig. 19. Performing the calculations with infinite fjords is a bit simpler, because there are fewer configurations, e.g., the configuration  $i=4$  would not appear in the first-order approximation for  $N=4$  [19].

#### D. Higher-order computations

As one increases  $N$  and the order of approximation  $O$ , the number of configurations increases exponentially, and it becomes harder to go over all of them manually. However, it is possible to construct a computer algorithm to perform the procedure described here. The main challenges are the automatic configuration recognition and automatic computation of the exact growth probabilities per configuration. In this section we explain the algorithm and report some of the important results.

The algorithm follows the method outlined in the examples of the previous sections, i.e., it goes over all the possible configurations of the interface. In the sample calculations we have initially made a list of all the possible configurations, called the index. Instead of doing this, the pro-

gram starts with only one configuration, namely the flat one (all the sites of the top row of the aggregate are occupied), which is indexed by  $j=1$ . This configuration grows with probability 1 to a new configuration that has one particle at the top row, while the row below it is fully occupied. This new configuration is inserted into the list of configurations with an index  $j=2$ . Therefore, the program sets  $E_{2,1}=1$  and  $p_{\text{up}}(1)=1$ . Then the program continues by handling the next configuration in the list, namely  $j=2$ . For each configuration, it solves the Laplace equations and calculates the growth probabilities. Each growth process may create a new configuration. The resulting configuration is first checked for consistency with the desired order  $O$ ; configurations which have  $\Delta m > O$  are truncated, as in Fig. 4. One then compares each “new” configuration with the existing list of configurations. If it does not exist in that list it is added at the end of the list, and indexed consecutively. If the index of the configuration that results from the growth process is  $i$  and the index of the initial configuration is  $j$  then the growth probability is inserted into the matrix element  $E_{i,j}$ . The total sum of all the upward growth probabilities of the initial configuration  $j$  is stored in  $p_{\text{up}}(j)$ . The main loop stops when the program finishes to process the last configuration in the index list. At this stage the Markovian evolution matrix  $\mathbf{E}$  is irreducible and closed, i.e.,  $\sum_i E_{i,j}=1$  for every  $j$ . Then the fixed point  $\mathbf{P}^*$  is calculated, by taking an initial vector and iterating  $\mathbf{E}$  on it many times until it converges (for very large matrices this is much faster than using any of the MATLAB library functions). The average upward growth probability is calculated using

$$\langle p_{\text{up}} \rangle^* = \sum_j P_j^* p_{\text{up}}(j), \quad (3.34)$$

the average density and the fractal dimension are then computed using the left-hand side of Eq. (2.20) and Eq. (2.22).

One of the challenges of the computer algorithm is the recognition of configurations. This recognition is important so that each growth process will be inserted into the evolution matrix  $E_{i,j}$  with the correct index  $i$  ( $j$  is the index of the configuration before growth). The recognition may be difficult because configurations that seem different may actually be equivalent. By equivalent we mean that they have the exact same set of transition (growth) probabilities. The solution to the Laplace equations is determined uniquely by the shape of the interface, therefore all of the configurations with the same external interface are equivalent. The description of the interface is not a trivial task though. We find that an efficient way to characterize an interface is by the set of empty sites that are connected to infinity. Of course, it is sufficient to specify only empty sites that are not higher than the highest particle in the aggregate, because all of the empty sites above it are connected to infinity. Figure 20 shows an example of two configurations that are not identical, but they have the same exterior contour. Both of them have a single empty site that is connected to infinity.

In order to reduce greatly the number of configurations it is advisable to take symmetry into account, i.e., all the configurations which can be obtained from one another using a rotation around the axis of the cylinder have the same growth probabilities and the same steady-state weights. The same is

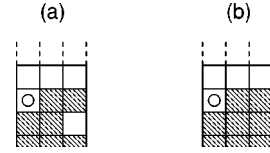


FIG. 20. Even though configuration (a) and (b) are not identical, they are equivalent because they have the same growth probabilities. Both configurations have the same external interface contour, which is characterized by the set of sites that are connected to infinity. In this example there is only one such site, which is not higher than the aggregate, and it is marked by a circle.

true for mirror images. Instead of taking all of them into account, we choose one as a canonical representative of the whole set of symmetric configurations.

The results are summarized in Table I. By comparing the approximations to accurate results from simulations, it seems that in order to obtain a relative accuracy of about  $10^{-3}$  one has to use at least an order of approximation of  $O=N-2$  (except for  $N=3$ , where one still has to use the second-order approximation). This becomes very difficult already for  $N=6$ , where in the fourth-order calculation there are 49 678 different configurations up to symmetry.

#### IV. DISCUSSION

This paper treats DLA as a Markov process. The Markov states are the possible shapes of the interface, and the Markovian evolution matrix  $\mathbf{E}$  is calculated analytically using exact solutions of the Laplace equations, with proper normalizations. We propose a truncation scheme that takes into account only a finite number of states. The states are ordered according to the maximal difference in height between the highest and lowest points on the interface,  $\Delta m$ , and in each order of truncation  $O$ , only the states with  $\Delta m \leq O$  are included. We justify this approach by the fact that the potential  $\Phi$  decays exponentially in deep fjords, and thus the shape of the interface in its deeper parts has very little effect on the growth probabilities. We perform this calculation for  $N=2$ , and verify that indeed it converges to the known analytic solution. We adopt the same approach for higher values of the width  $N$ , between 3 and 7, and calculate the average density  $\rho$  in good agreement with simulations. The fact that the number of configurations grows exponentially with  $N$  and with  $O$ , makes the computation less effective than simulation for large  $N$ .

We observe that the method converges as a function of  $O$ , also for higher values of  $N$ . Let us denote the calculated average steady-state density of an aggregate of width  $N$  in the  $O$ 'th-order approximation by  $\rho_c(N, O)$ . We observe that  $\rho_c(N, O)$  converges to a finite limit very rapidly as a function of  $O$ . In fact, a relative accuracy of  $10^{-3}$  is achieved for  $O=N-2$  (except for  $N=3$ ). This enables us to obtain accurate results for  $3 \leq N \leq 6$ . The drawback of this method is that the number of configurations diverges exponentially with  $O$  and  $N$ , and therefore it is possible to perform the calculations only for relatively low  $N$ 's and  $O$ 's. Our computer was strong enough to perform the calculation only in the third-order approximation for  $N=7$ , and therefore the result for  $N=7$  is not very accurate. One would hope that it may be possible to perform low-order approximations for

large  $N$ 's and then extrapolate, in order to estimate the results for large  $O$ 's. Indeed, it is reasonable to conjecture the scaling law  $\rho_c(N, O) = \rho(N)f(N/O)$ , where  $\rho(N)$  is the exact ( $O \rightarrow \infty$ ) density, as a function of  $N$ , and  $f(N/O)$  is a universal scaling function that obeys  $\lim_{x \rightarrow 0} f(x) = 1$ . Our investigation shows that in spite of the fact that the conjecture is not very accurate for  $O=1$  and  $O=2$ , it is quite good for higher values of  $O$ , and presumably also for higher values of  $N$ . This scaling relation may help to perform the extrapolation  $O \rightarrow \infty$  for higher values of  $N$ . Paradoxically, it is very hard to obtain data points for large  $N$ 's and  $O$ 's, and thus to extract the scaling function accurately. Thus we are unable to make the extrapolation even for  $N=7$ , and we estimate  $\rho(N)$  by the highest-order approximation available. However, we suggest an alternative way to obtain  $\rho_c(O, N)$ , namely by simulation: it is possible to perform a regular DLA simulation in cylindrical geometry, only that one has to keep the  $O$ 'th row below the highest particle in the aggregate constantly filled. Measuring the average density of the aggregate in such a simulation would approximate  $\rho_c(N, O)$ . This simulation would be faster than a regular simulation, because particles would stick faster, due to the fact that they have less free space. This study would perhaps yield the scaling function  $f(N/O)$ , and enable extrapolation of lower order approximations for higher  $N$ 's, should anyone venture to perform them on more powerful computers. In light of this discussion we suggest a more efficient way to perform DLA simulations in cylindrical geometry. We argue that one can obtain a relative accuracy of  $10^{-3}$  if one follows just the  $N-2$  topmost rows of the aggregate. This should save some time, because the diffusing particle would stick faster, and it would also require less memory. This is not to say that it is sufficient to grow the aggregate until it reaches a height of  $N-2$ , but rather, to perform many more growth processes, and each time the aggregate reaches a height of  $N-1$ , truncate the bottom row.

We also discuss the temporal rate of convergence of the system to its steady state. In this context we find that there is an exponential convergence to the steady state, and we calculate the characteristic time constant  $\tau$ . This is demon-

strated using the simple model of the frustrated climber. The convergence is described in terms of the eigenvalues of the Markovian matrix, and in terms of the infinite shift-down operator.

Considering the fractal dimension, Pietronero *et al.* suggested that  $\rho(N) = N^{D-d}$ , as mentioned in Eq. (2.21). In principle, one should always include an amplitude and finite size corrections of the form

$$\rho(N) = AN^{-\alpha}(1 + B/N + \dots), \quad (4.1)$$

where  $\alpha = d - D$ , and  $A$  and  $B$  are constants. The second term appearing in Eq. (4.1) is a correction to scaling term. Generally, there is an infinite sum of such terms with higher negative powers of  $N$ . Because we have data only for small values of  $N$ , these correction terms may be large, but since we have only a few accurate data points ( $\rho(N)$  for  $N=2, 3, \dots, 6$ ), we try to extract the parameters  $\alpha$ ,  $A$  and  $B$  only, and not higher-order terms. Using the three results for  $N=4, 5, 6$ , we determine the three unknown parameters to be  $A=0.82$ ,  $B=0.35$ , and  $\alpha=0.362$ , hence  $D=1.64$ . The deviation from the well known value of  $D=1.66$  can be attributed to systematic error due to the omission of higher-order finite size correction terms. We fit simulation data [19] for  $N=3, 4, 5, 6, 7, 32, 48, 64, 96, 128$ , to a higher-order approximation  $\rho(N) = AN^{-\alpha}(1 + B/N + C/N^2)$ , and find that  $C = -0.205$ ,  $B=0.561$ ,  $A=0.761$ , and  $\alpha=0.339$ , which means that  $D=1.661$ . The maximum relative error of the fit is  $1.2 \times 10^{-3}$ , and the average relative error is  $1.0 \times 10^{-3}$ , which is in good agreement with estimated accuracy of the simulations.

#### ACKNOWLEDGMENTS

We wish to thank Barak Kol and A. Vespignani for helpful discussions. We also wish to thank Yiftah Navot for helping with the computer program, by suggesting more efficient data structures and algorithms. We thank Nadav Schnerb for offering the frustrated climber metaphor. This work was supported by a grant from the German-Israeli Foundation (GIF).

- 
- [1] T.A. Witten and L.M. Sander, Phys. Rev. B **27**, 5686 (1983).  
 [2] B. Mandelbrot, *The Fractal Geometry of Nature* (Freeman, New York, 1982).  
 [3] J. Feder, *Fractals* (Plenum, New York, 1988).  
 [4] L. Niemeyer, L. Pietronero, and H.J. Wiesmann, Phys. Rev. Lett. **52**, 1033 (1984).  
 [5] P. Bak, C. Tang, and K. Wiesenfeld, Phys. Rev. Lett. **59**, 381 (1987); Phys. Rev. A **38**, 364 (1988).  
 [6] A. Erzan, L. Pietronero, and A. Vespignani, Rev. Mod. Phys. **67**, 545 (1995).  
 [7] H. Gould, F. Family, and H.E. Stanley, Phys. Rev. Lett. **50**, 686 (1986).  
 [8] T. Nagatani, Phys. Rev. A **37**, 3514 (1988); **38**, 2632 (1988).  
 [9] X.R. Wang, Y. Shapir, and M. Rubinstein, Phys. Rev. A **39**, 5974 (1989); J. Phys. A **22**, L507 (1989).  
 [10] M.B. Hastings and L.S. Levitov, Physica D **116**, 244 (1998).  
 [11] M.B. Hastings, Phys. Rev. E **55**, 135 (1997).  
 [12] B. Kol and A. Aharony (unpublished).  
 [13] R. Cafiero, L. Pietronero, and A. Vespignani, Phys. Rev. Lett. **70**, 3939 (1993).  
 [14] L. Pietronero and H.J. Wiesmann, J. Stat. Phys. **36**, 909 (1984).  
 [15] B. Kol and A. Aharony, Phys. Rev. E **58**, 4716 (1998).  
 [16] In [14] there are functions of the form  $a(j) = a(\infty) + x_0 e^{-\alpha j} (1 + x_1 e^{-\beta j} + x_2 e^{-2\beta j} + \dots)$ , where  $a(\infty), x_0, \alpha > 0, \beta > 0, x_1, x_2, \dots$  etc. are arbitrary constants. For the present model, the average converges exponentially  $\langle a \rangle(t) = \langle a \rangle^* + p^t \sum_{j=0}^{\infty} a(j+t) v_j(0) = \langle a \rangle^* + x_0 p^t e^{-\alpha t} [f_0 + f_1 e^{-\beta t} + f_2 e^{-2\beta t} + \dots]$ , where  $\langle a \rangle^* \equiv \sum_{j=0}^{\infty} q p^j a(j)$ , and  $f_i = x_i \sum_{j=0}^{\infty} e^{-(\alpha+i\beta)j} v_j(0)$ . Note that the constant  $a(\infty)$  does not affect the rate of convergence.  
 [17] L.A. Turkevich and H. Scher, Phys. Rev. Lett. **55**, 1026 (1985).  
 [18] L. Pietronero, A. Erzan, and C. Evertsz, Physica A **151**, 207 (1988).  
 [19] B. Kol and A. Aharony (unpublished).